Research Article Vol. 30, No. 5 / 28 Feb 2022 / Optics Express 6970
Optics EXPRESS

Third-order optical nonlinearities of exfoliated Bi_2Te_3 nanoparticle films in UV, visible and near-infrared ranges measured by tunable femtosecond pulses

VYACHESLAV V. KIM,[1] ARTURS BUNDULIS,[2] VIKTOR S. POPOV,[3] NIKOLAY A. LAVRENTYEV,[3] ANNA A. LIZUNOVA,[3] IVAN A. SHUKLOV,[3] VLADIMIR P. PONOMARENKO,[3] JURGIS GRUBE,[2] AND RASHID A. GANEEV[1,4,5,*]

[1]*Laboratory of Nonlinear Optics, Institute of Astronomy, University of Latvia, LV-1004 Riga, Latvia*
[2]*Institute of Solid State Physics, University of Latvia, Kengaraga 8, Riga LV-1063, Latvia*
[3]*Moscow Institute of Physics and Technology (National Research University), Dolgoprudny 141701, Russia*
[4]*Department of Physics, Voronezh State University, Voronezh 394006, Russia*
[5]*Tashkent Institute of Irrigation and Agricultural Mechanization Engineers, National Research University, Kori Niyozov Street 39, Tashkent 100000, Uzbekistan*
[*]*rashid.ganeev@lu.lv*

Abstract: We characterize the nonlinear optical properties of synthesized Bi_2Te_3 nanoparticle-contained thin films using the tunable femtosecond laser in the spectral range of 400–1000 nm. These nanoparticles possess a strong saturable absorption and positive nonlinear refraction (-6.8×10^{-5} cm W^{-1} in the case of 500 nm, 150 fs probe pulses, and 3×10^{-10} cm^2 W^{-1} in the case of 400 nm, 150 fs probe pulses, respectively). The spectral, intensity, and temporal variation of saturable absorption and nonlinear refraction of the thin films containing exfoliated Bi_2Te_3 nanoparticles are discussed.

1. Introduction

Nonlinear optical properties of various nanoparticles (NPs) took attention due to their potential applications in various areas of optoelectronics and photonics. Among numerous NPs studied during the last few decades, the exfoliated small-sized structures can be of especial interest due to their use in mode-locking and Q-switching of lasers, as well as for the applications as efficient emitters of the coherent short-wavelength radiation during high-order harmonics generation. The latter option can be realized during ablation of bismuth telluride (Bi_2Te_3) NPs contained targets and propagation of laser pulses through the plasmas containing those nanostructures.

The interest in the exfoliated Bi_2Te_3 NPs, apart from the above-mentioned areas, is attributed to the improvement of the characteristics of IR radiation detectors. Bi_2Te_3 was used as a photosensitive component in the form of epitaxial layers or individual NPs: nanowires or nanoplates. Correspondingly, the use of topological insulators, and in particular bismuth telluride, is actively developing for applications in various areas of electronics. The thin films comprising such NPs are of special interest since they can be incorporated inside the master oscillators to modify the temporal shape of the emitted radiation. Another interesting potential application could be the generation of harmonics after the propagation of short laser pulses through such structures.

All the above-mentioned potential applications of exfoliated Bi_2Te_3 NPs thin films require the study of their third-order nonlinear optical properties. Saturable absorption (SA), as a prerequisite of application of these nanostructures for the mode-locking and Q-switching of lasers, is one of the most important parameters requiring accurate measurements along the broad spectral range to

#449490 https://doi.org/10.1364/OE.449490
Journal © 2022 Received 24 Nov 2021; revised 16 Jan 2022; accepted 19 Jan 2022; published 16 Feb 2022

Optics EXPRESS

provide the opportunity in optimization of the application of those thin films for above-mentioned tasks. The same can be said about the nonlinear refraction (NR) in such thin films. The Kerr-related processes can either amend or diminish the potential applications of Bi_2Te_3 NPs thin films as Kerr lens modulators depending on the wavelength of laser radiation. The analysis of these properties is also required for the prediction of the behavior of the laser-induced plasmas containing Bi_2Te_3 NPs during high-order harmonics generation.

First attempts to analyze the low-order nonlinear optical properties of Bi_2Te_3 NPs were reported in [1] where the growth of transmittance of bismuth chalcogenide nanoplates was analyzed. In [2], the mode-locking of lasers using Bi_2Te_3 topological insulator nanoparticles was demonstrated. The potential applications of these species in ultrafast photonics were analyzed in [3]. The nonlinear refractive index (γ), nonlinear absorption coefficient related with saturable absorption (β_{SA}), and saturation intensity (I_{sat}), as well as the role of carrier transfer in layered Bi_2Te_3 topological insulators, were analyzed in [4,5]. The nonlinear absorption (NA) effect in the films containing bismuth telluride was reported in [6]. Broadband nonlinear optical response in Bi_2Te_3 nanosheets was reported in [7] where the wavelength-dependent third-order nonlinear optical response of Bi_2Te_3 was experimentally reported and the third-order nonlinear refractive index was measured with a peak value of 2×10^{-8} cm^2 W^{-1} at a wavelength of 1.93 μm. All those nonlinear optical studies were carried out using pico- and femtosecond laser pulses. Most of them were concentrated on the nonlinear optical absorption studies, while the fast Kerr-related mechanism of nonlinear refraction was considered only in Ref. [7]. The studies related with the application of the nanosecond pulses in two spectral ranges (532 and 1064 nm) to determine the role of thermal effect in Bi_2Te_3 NPs and compare it with the fast, Kerr-related processes of NR were reported in [8]. Additionally, the application of 10 ns pulses allowed observation of SA. Meanwhile, to the best of our knowledge, no studies were reported about the γ, β_{SA}, and I_{sat} of thin (of a few tens nanometers) films containing such topological insulators along a broad range using tunable femtosecond pulses.

In this paper, we present the results of characterization of the nonlinear optical properties of synthesized Bi_2Te_3 nanoparticles-contained thin films using the tunable femtosecond laser in the range of 400–1000 nm. We demonstrate that these nanoparticles possess strong saturable absorption and positive nonlinear refraction. We present the spectral, intensity, and temporal variation of SA and NR in the thin films containing exfoliated Bi_2Te_3 nanoparticles.

2. Experimental

2.1. Preparation of samples

The details of Bi_2Te_3 NP synthesis are presented elsewhere [8]. Briefly, exfoliated bismuth telluride NPs consisted of repeated quintuple layers (QL) comprising five atomic layers in the sequence $Te^{(1)}$ – Bi – $Te^{(2)}$ – Bi – $Te^{(1)}$. Those atomic layers approximately correspond to the dimension of 1 nm. It is fundamentally possible to delaminate the bulk bismuth telluride to the maximum thickness of 1-1.5 nm. Such weak bonds make it possible to obtain thin layers of Bi_2Te_3 using simple exfoliation methods without additional surfactants. Previous studies allowed obtaining stable dispersions of bismuth telluride NPs in alcohols using a simple laboratory ultrasonic bath [9,10]. Suspension of 2D Bi_2Te_3 NPs 0.01M was made by liquid-phase exfoliation (LPE) of Bi_2Te_3 powder in butanol-1 with sonication bath (650W) for 8 hours at 30-45°C. This Bi_2Te_3 suspension was used for coating of 1-mm thick silica glass substrates by dip-coating method with different withdrawal speed (1.3 and 4.7 mm/h) immediately after LPE.

The coating was scratched to see the thickness of the films. Atomic force microscope analysis provided 60-100 nm thickness for the sample prepared by the slower speed of dip-coating and 40-50 nm for faster withdrawal speed. In our experiments, we used 60 nm thick films.

Drop-casting of Bi_2Te_3 nanosheets dispersions in alcohol on substrate results in the preferred nanosheets orientation along the (001) plane [11]. The absorption spectrum of the studied

Optics EXPRESS

film is shown in Fig. 1(a). JEM-2100 was used for transmission electron microscopy (TEM) of the fresh exfoliated Bi_2Te_3 suspension. TEM images confirm the crystalline structure of obtained thin-layered Bi_2Te_3 particles, which also corroborates with XRD results. Each particle represented an aggregate of several smaller thin 2D-crystallites with an average size of about 10 nm. The sizes of aggregates varied in the range of 75 - 150 nm (inset in Fig. 1(a)).

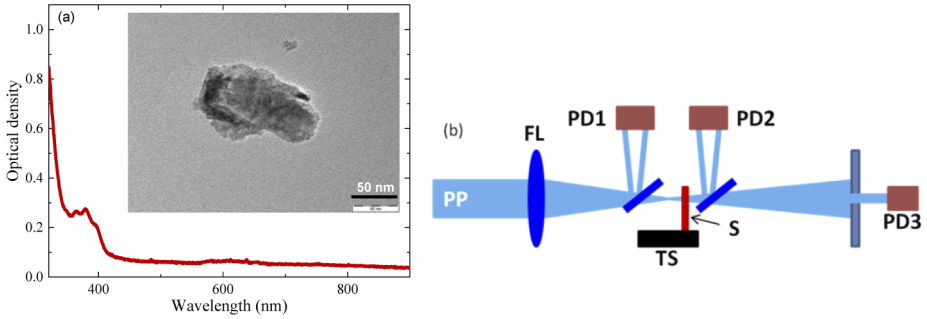

Fig. 1. (a) Optical density of Bi_2Te_3 NPs film. Inset: TEM of single Bi_2Te_3 NP. (b) Z-scan scheme. PP, probe pulse (150 fs, 400–1000 nm); FL, focusing lens; PD1 – PD3, photodiodes (see text); S, sample (60-nm thick NP film on the 1-mm thick glass slide); TS, translating stage.

The prepared samples were stored under atmospheric conditions and normal humidity. Due to more than 300 hours' time gap between sample preparation and Z-scan measurements, the surface of Bi_2Te_3 nanosheets may have not more then 1.3-1.5 nm oxidized layer from the top side in accordance with the data reported in [12].

2.2. *Z-scan and fitting procedure*

The tunable laser source (ORPHEUS-HP + PHAROS PH2 femtosecond laser) provided the probe pulses (PP) during these studies. The 150 fs pulses at 500 kHz repetition rate allowed the tuning along the 400–1200 nm spectral region. The standard Z-scan technique was used for the studies of the nonlinear optical properties of our films (Fig. 1(b)). Laser radiation was focused with a 110 mm focal length spherical lens. The sample (60-nm thick film of Bi_2Te_3 NPs deposited on the 1-mm thick silica glass plate) was moved along the z-axis through the focal plane of the spherical lens. The propagated radiation was measured by photodiodes PD2 (open-aperture (OA) scheme) and PD3 (closed-aperture (CA) scheme). PD1 was used to allow the determination of the normalized transmittances in the case of OA and CA Z-scan schemes.

Special attention was paid to the CA Z-scans. To obtain them, the 1-mm aperture was fixed at a distance of 200 mm from the focal plane, behind which the PD3 was located. The ratio of the transmitted radiation registered by this photodiode and the incident radiation registered by PD1 placed prior to the focusing lens was taken as the normalized transmission. Away from the focal point, where nonlinear processes do not occur, the normalized transmission was 1. This made it possible to avoid the influence of instability of the laser radiation on the results obtained. Each point on the experimental dependencies corresponds to an average of 20 measurements. The scheme with CA allowed the determining the sign and value of the nonlinear refractive index of the Bi_2Te_3 NPs film. The OA scheme allowed determination of the NA of samples. The CA Z-scan scheme was calibrated using the known value of the nonlinear optical refraction of carbon disulfide. The error bars of the definition of the absolute values of nonlinear optical parameters were estimated to be ±30% due to the uncertainty in the measurements of the intensities of laser pulses in the focal plane.

Optics EXPRESS

The most pronounced processes during these studies were the SA and NR in the case of femtosecond pulses. The fitting of the experimental CA data was carried out using the relation [13]:

$$T = 1 + \frac{2(-\rho x^2 + 2x - 3\rho)}{(x^2 + 9)(x^2 + 1)}\Delta\Phi_0. \quad (1)$$

Here $x = z/z_0$, z_0 is the Rayleigh length of the focused radiation, $z_0 = \pi(w_0)^2/\lambda$, w_0 is the beam waist radius, λ is the wavelength of the probe radiation, $\rho = \beta/2k\gamma$, $k = 2\pi/\lambda$, $\Delta\Phi_o = k\gamma I_0 L_{\text{eff}}$, I_0 is the laser radiation intensity in the focal plane, $L_{eff} = [1\text{-exp}\ (-\alpha_0 L)]/\alpha_0$ is the effective length of the sample, α_0 is the linear absorption coefficient, and L is the thickness of the studied film.

To fit the OA data and determine the nonlinear absorption coefficient responsible for SA (β_{SA}) we used the relation [14]:

$$T \approx 1 - \frac{p(x)}{8^{0.5}} \quad (2)$$

where $p(x) = \beta_{SA} I_0 L_{\text{eff}} \left[1 + x^2\right]^{-1}$.

We also determined the saturation intensity, which was defined as the optical intensity required for the two-fold increase of the normalized transmittance in the case of SA.

3. Results

3.1. Nonlinear absorption

The saturable absorption was a dominating NA effect during the whole set of these studies. We did not observe the positive nonlinear absorption. Neither two-photon absorption nor reverse saturable absorption played a significant role in the case of application of the 150 fs PP varying by energy (intensity) between 5 and 100 nJ (6×10^8–1.2×10^{10} W cm^{-2}). The analysis of the OA Z-scans along the whole range of spectral variations of the PP allows concluding about the spectral dependence of β_{SA}. The microscopic analysis of films after Z-scans did not show the appearance of holes. The above-mentioned used intensities during these studies were far less than the breakdown threshold of these films (~8×10^{10} W cm^{-2}), thus pointing out the involvement of SA in the bleaching of the studied samples. The application of notably stronger pulses (700 nJ) led to the appearance of visible damage on the surface of the film.

In accordance with the model of SA, the relaxation rate of excitations does not depend on the intensity. The absorption rate A is determined by the parameter $A = \alpha_0 /(1 + I/I_{sat})$. Here I is the variable intensity along the Z-axis during focusing of laser radiation. α_0 and I_{sat} are related to the concentration of the active centers in the medium, the effective cross-sections, and the lifetime of the excitations.

Figure 2 shows a set of OA Z-scans of the 60-nm thick film of Bi_2Te_3 NPs deposited on the 1-mm thick silica glass plate. All scans were carried out at the same energy of 150 fs pulses (25 nJ, $I_0 = 3\times10^9$ W cm^{-2}). The tuning of PP was performed with a step of 100 nm. One can see that the bleaching of the film was steadily increased with a decrease of the wavelength from 1000 to 500 nm. A further shift of wavelength to 400 nm led to a decrease of the peak of the OA Z-scan, which could be attributed to the growing influence of the linear absorbance in this spectral region (see Fig. 1(a)).

The fitting of OA Z-scans using Eq. (2) was used for defining the nonlinear absorption coefficient related to the saturable absorption. Figure 3 shows the experimental data of the Z-scans of the film and pure silica glass and the fitting curve of the former scan in the case of 25 nJ, 600 nm pulses. We did not see any nonlinear effect in the pure silica glass, though it was more than 10^4 times thicker than the Bi_2Te_3 NPs film. The fitting using Eq. (2) allowed determining the parameter p and correspondingly β_{SA} [$\beta_{SA} = -(5 \pm 1.5)\times10^{-5}$ cm W^{-1})]. The error bars for these measurements were estimated to be 30%. This parameter was varied between -1.5×10^{-5} cm W^{-1} (at 1000 nm) and -6.8×10^{-5} cm W^{-1} (at 500 nm), so the bleaching significantly depended on the

Optics EXPRESS

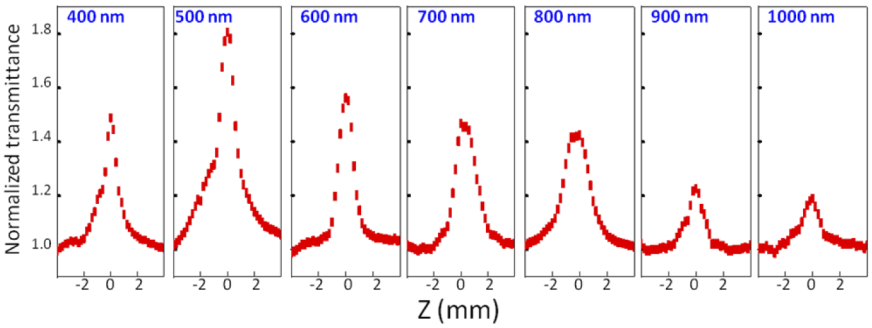

Fig. 2. Open-aperture scans of film using 150 fs, 25 nJ pulses in the range of 400–1000 nm.

wavelength of PP. The corresponding saturation intensity was determined to be $I_{sat} = 1.5\times10^{10}$ W cm^{-2} in the case of 400 nm PP and $I_{sat} = 3.2\times10^{10}$ W cm^{-2} in the case of 900 nm PP. One can see that thin films containing exfoliated Bi_2Te_3 NPs possess relatively low values of saturated intensities. The low-I_{sat} saturable absorbers may allow the formation of low-power femtosecond laser sources. The saturation intensity of light at which the extinction coefficient is reduced by a factor of 2 is an important parameter of such lasers. Among the quantum dots used for the modern passively mode-locked and Q-switched lasers [15–17], the studied Bi_2Te_3 NPs films possess the smallest I_{sat}.

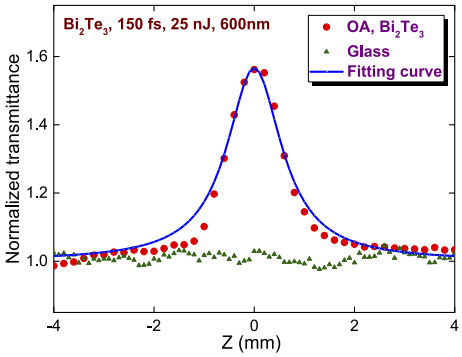

Fig. 3. Open-aperture Z-scan of film (filled red circles) and glass (filled green triangles) using 25 nJ, 600 nm pulses. Solid blue curve shows the fitting of experimental data using Eq. (2).

SA does not directly follow the spectral absorption dependence since the former process depends on different factors related to the structure of energy levels of the studied material. Our studies show that Bi_2Te_3 NPs films can be useful as saturable absorbers in the laser cavities for passive Q-switching and mode-locking.

The possibility of the dynamic scattering of the probe pulses by Bi_2Te_3 NPs was recently studied using 10 ns pulses [8]. Those studies did not observe the nonlinear scattering in the case of 532 nm probe pulses. No valley was observed during our OA Z-scans as well, which point out the insignificance of this process in the studied films in the case of femtosecond PP.

The microscopic analysis of Bi_2Te_3 NPs films after Z-scans did not show the appearance of holes, which is related to the use of weak intensities of the femtosecond pulses. The used intensities during these studies were far less than the breakdown threshold of these films

Optics EXPRESS

thus pointing out the involvement of SA in the bleaching of the studied films rather than the drilling-related growth of transmittance of the film in the vicinity of the focal plane.

3.2. Nonlinear refraction

NR was observed only in the shorter-wavelength region. Figure 4 shows the OA, CA, and the division (CA/OA) of these two scans. The fitting of CA/OA using Eq. (1) allowed determining the nonlinear refractive index of the studied Bi_2Te_3 NPs film using 150 fs, 400 nm, 50 nJ PP. The discrepancy between the fitting and experimental CA/OA curve shown in Fig. 4 can be attributed to some asymmetric (slightly elliptical) shape of the used beam in the focal area (see the discrepancy in the case of the negative and positive values of z). Similar discrepancies between theory and experiment were obtained in the case of other fittings performed during our studies.

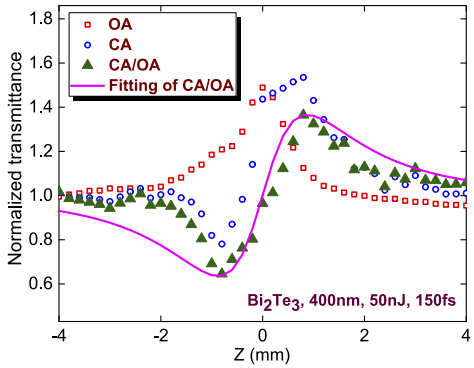

Fig. 4. Open-aperture (OA, empty red squares), closed-aperture (CA, empty blue circles), CA/OA (filled green triangles), and fitting (CA/OA, solid magenta, Eq. (1)) Z-scans of Bi_2Te_3 NPs film. 150 fs, 400 nm, 50 nJ radiation was used as PP.

In all our CA experiments we observed the positive nonlinear refraction. The application of 150 fs PP even at a high pulse repetition rate (500 kHz) did not reveal the thermal lens formation resulting in observation of the self-focusing in the shorter-wavelength region (400 nm). Notice that in this region the linear absorption is relatively large (OD = 0.2, Fig. 1(a)). Nevertheless, the thin film did not form a thermal lens due to the accumulative effect. Further, in the case of relatively long pulses, the molecular Kerr-related nonlinearities can prevail over electronic Kerr-related processes. Commonly, the former refractive nonlinearities demonstrate self-defocusing properties. The prevalence of molecular nonlinearities related to the reorientational mechanisms may play important role in the picosecond timescale over the Kerr-related electronic nonlinearities caused the observation of the negative sign of the effective nonlinear refractive index. However, in the case of 150 fs PP, the positive sign of γ was observed along the whole range of studies of this effect (400–700 nm).

One can exclude the NA from the CA experimental results via the CA/OA operation. We used such a possibility in retrieving the purely nonlinear refractive effect. Notice that the CA/OA operation is a useful tool once one determines those scans in a single set of measurements. The fitting of CA/OA allowed determining the nonlinear refractive index [$\gamma = (3 \pm 1) \times 10^{-10}$ cm^2 W^{-1}] of the film using 400 nm PP.

The nonlinear refractive index significantly decreased with the growth of the wavelength of PP compared with the value measured at $\lambda = 400$ nm. Particularly, it was dropped by a factor of 5 at $\lambda = 600$ nm and by a factor of 150 at $\lambda = 800$ nm.

The attractive feature of small-sized species is their variable response related to the size effect, when the quantum confinement starts playing a decisive role in the case then the local field

Optics EXPRESS

related effects enhance the nonlinear optical response of tiny particles, i.e. those which radius is less than the Bohr radius of the studied material. This is an interesting phenomenon; however, we did not analyze the nonlinear optical parameters for different particles, since the sizes of our NPs were notably larger than the anticipated Bohr radius of these species. Correspondingly, we could not expect observation of quantum confinement-related effect once using the relatively large particles.

Our studies show that further characterization of Bi_2Te_3 NPs film in femtosecond timescale is necessary to determine the interplay between self-phase modulation and group velocity dispersion, which can play a significant role in altering the peak irradiance inside the sample resulting in strongly influenced output transmission.

4. Discussion

The wavelength- and geometry-dependent mechanisms of the NA in the Bi_2Te_3 NPs are quite sophisticated processes. This problem has been analyzed in [1–7]. Those studies offered different scenarios in explanation of the observed peculiarities of NA in these species. We refer to those studies while discussing below some peculiar features of the spectral dependences of NA and NR in the studied bismuth telluride NPs.

Figure 5(a) comprises our studies of NA and NR using tunable PP. One can see the disappearance of self-focusing in the studied films at wavelengths above 800 nm. Meanwhile, NA showed an insignificant decrease with the growth of the wavelength of PP. By any means, the shorter-wavelength PP allowed increasing the nonlinear optical response of Bi_2Te_3 NPs film.

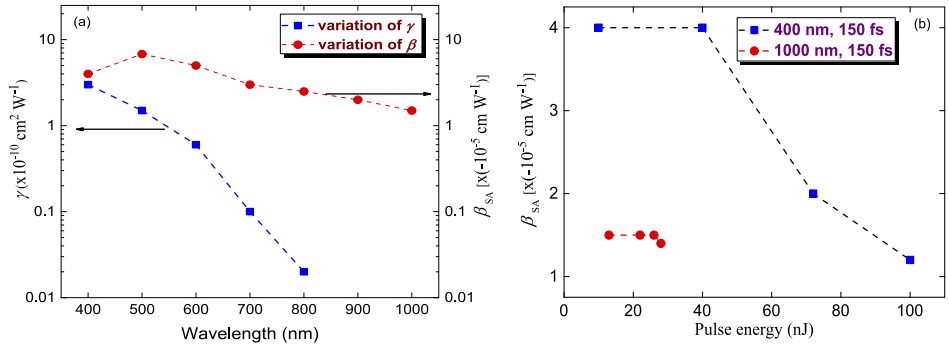

Fig. 5. (a) Variations of the nonlinear refractive index (filled blue square) and SA nonlinear absorption coefficient (filled red circles) of Bi_2Te_3 NPs film in the 400–1000 nm spectral range. (b) Energy-dependent variations of the nonlinear absorption coefficient of Bi_2Te_3 NPs film in the case of 400 nm (filled blue squares) and 1000 nm (filled red circles) PP.

The PP energy dependence of β_{SA} is presented in Fig. 5(b) in the case of two wavelengths of the PP. In the case of 400 nm PP, it was notably decreased (from -4×10^{-5} cm W^{-1} to -1.2×10^{-5} cm W^{-1}) with the growth of pulse energy. Meanwhile, in the case of 1000 nm pulses, this decrease was not observed, though we measured this parameter in a narrow range.

Finally, we compared the nonlinear optical properties of Bi_2Te_3 NPs film measured by 150 fs and 10 ns pulses. The latter data were reported in Ref. [8]. In the following graphs, we refer to those studies while providing the quantitative comparison in these two cases. Figure 6(a) presents the comparison of NA and NR of films at two spectral ranges (500 and 1000 nm) measured using 150 fs and 10 ns pulses. The NA related with SA was approximately the same, with a factor of ~3 (empty and filled red squares).

Meanwhile, there is a large difference between the γ measured by nanosecond and femtosecond pulses (empty and filled blue squares). The γ measured using 10 ns pulses was three orders of

Optics EXPRESS

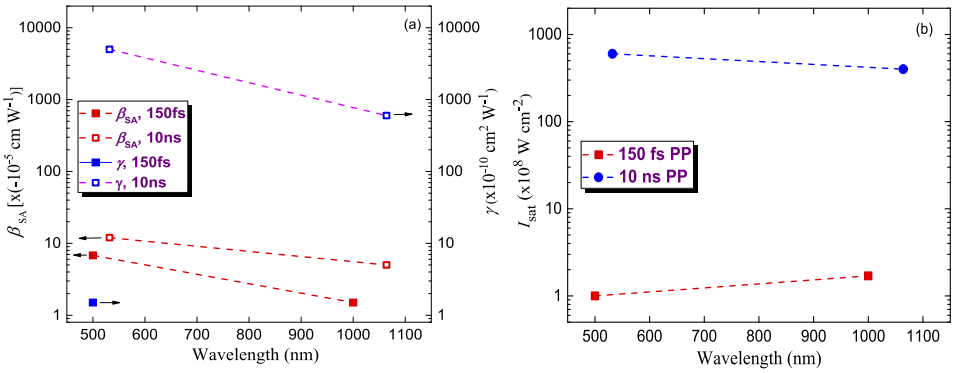

Fig. 6. (a) Dependencies of γ (150 fs: filled blue square; 10 ns: empty blue squares) and β_{SA} (150 fs: filled red squares; 10 ns: empty red squares) at two spectral ranges of the PP of different duration (150 fs and 10 ns). Data of γ and β_{SA} for 10 ns probe pulses were taken from Ref. [8]. (b) Dependencies of saturated intensity (150 fs: filled red squares; 10 ns: filled blue circles) at two spectral ranges of the PP of different duration (150 fs and 10 ns). Data of I_{sat} for 10 ns probe pulses were taken from Ref. [8].

magnitude larger than the one measured by 150 fs pulses. One can anticipate in this case the crucial involvement of the molecular reorientation effect in the case of longer pulses. Additionally, a significant difference was observed in the case of the saturated intensities in both spectral regions (Fig. 6(b)). In that case, I_{sat} measured by femtosecond pulses was almost three orders of magnitude lower compared with the measurements carried out by nanosecond pulses. This attractive feature of Bi_2Te_3 NPs film can be applied in the mode-lockers and Q-switchers. Further, I_{sat} insignificantly increased with the growth of the wavelength of 150 fs PP (filled red squares, Fig. 6(b)).

The nonlinear optical properties of synthesized exfoliated Bi_2Te_3 NPs films can find various applications in optoelectronics and nanophotonics [18]. The optical and optoelectronic properties of topological insulators, like Bi_2Te_3 NPs layers, are extremely attractive since, while possessing the unique energy band, they demonstrate wideband nonlinear saturable absorption. These properties allow for the application of such topological insulators for various nonlinear devices, like optical Q-switchers, mode-lockers, and wavelength converters [19–23].

The surface oxidation of Bi_2Te_3 NPs to Bi_2O_3 and TeO_2 may lead to the changes in the properties of the films. It is shown in [24] how the oxidation may modulate the refractive index and extinction coefficient of Bi_2Te_3 thin films in the visible and near infrared ranges. Meanwhile, it is rather difficult to judge about the influence of this process on the nonlinear optical parameters of these NPs.

Below we address the details allowing distinguishing our spectral-dependent studies with regard to the measurements of the optical nonlinearities of bismuth telluride nanocrystals at some fixed wavelengths reported so far. Though some studies report the fabrication of Bi_2Te_3 nanostructures with a fine plate-like shape and a particle size in the range of 80 nm (for example [25]), a few reports underline their nonlinear optical parameters. Particularly, the nonlinear optical properties of these species at three fixed wavelengths in the border between the near-infrared and mid-infrared (1562 and 1930nm), as well as at $\lambda = 800$ nm, have been investigated [7]. The third-order nonlinear refractive index was measured with a peak value of $\sim 2\times10^{-8}$ cm^2 W^{-1} at a wavelength of ~2 μm by both OA and CA Z-scans with ultrafast laser in picosecond and femtosecond timescales. They have shown significant growth of the self-focusing in the ~2 μm range compared with the use of the 0.8 μm PP ($\sim 1\times10^{-10}$ cm^2 W^{-1}). Notice that the former parameter was obtained at approximately the same pulse duration (100 fs) as in our case (150 fs),

Optics EXPRESS

while the latter value was measured using the 800 nm, 3 ps pulses. The difference in experimental conditions makes it difficult to compare these parameters due to the potential involvement of additional processes in the case of longer pulses. Meanwhile, our studies were extended to the region spanning from 400 to 800 nm using the same pulse duration (150 fs). We showed that in the visible and, especially, UV range, the nonlinear refractive index of Bi_2Te_3 NPs is steadily increasing (i.e. by two orders of magnitude at $\lambda = 400$ nm compared with the 800 nm region, see Fig. 5(a)). Thus our study demonstrates a significant modification of the Kerr-related response of these NPs in the 400-800 nm spectral range. As for the saturable absorption in these NPs, the saturation intensity of Bi_2Te_3 NPs reported in [7] was $I_{sat} = 1\times10^{10}$ W cm^{-2} in the case of the 800 nm, 100 fs PP, which was four times less than in our case (800 nm, 150 fs). This difference can be related to the difference in the concentrations of NPs in the two experiments.

The dynamics of saturable intensity at different conditions of excitation of the Bi_2Te_3 NPs was reviewed in [4]. With respect to this parameter of the studied species, low intensities from several W cm^{-2} to several kW cm^{-2} as well as high intensities from several MW cm^{-2} to GW cm^{-2} have been reported. In general, the low and high saturation intensities are related to the contribution from the bulk state and surface state, respectively. In addition, a two-photon absorption effect in Bi_2Te_3 has been reported [4] through a Z-scan measurement using the low and high pulse energy regions corresponding to the measurement of the evolution of the optical nonlinear transmittance for this material. Those studies were carried using the Q-switched solid-state laser with a repetition rate of 100 Hz and a pulse width of 300 ns. Such long pulses allow the observation of two-photon absorption alongside the saturable absorption, contrary to the case of the ultrashort laser PP, which demonstrated only a purely saturable absorption in Bi_2Te_3 NPs. Notice that neither our studies nor the other reports using femtosecond probe pulses demonstrated the two-photon absorption in the studied material in the case of the moderate (1×10^9 W cm^{-2}) intensities of the PP. Additionally, the long (300 ns) pulses led to the self-defocusing in the Bi_2Te_3 NPs, which is attributed to the thermal-lens effect contrary to the Kerr-related self-focusing observed in our and others studies using the femtosecond pulses.

The role of carrier transfer in the optical nonlinearity of graphene/Bi_2Te_3 heterojunctions was analyzed in [5]. Though the refereed study was mostly related to the potential applications of such structures for the mode-locking of lasers, the optical limiting effect was attributed to the positive nonlinear absorption at small intensities of 40 fs pulses ($\sim1\times10^8$ W cm^{-2}), which was then transformed to SA at higher laser intensities.

Thus the duration of PP pulses plays a decisive role in the dynamics of the nonlinear optical processes in bismuth telluride NPs. In [6], the 4 ns pulses were used for the measurements of the variations of the nonlinear absorption coefficient of this material. The normalized transmittance curves of Bi_2Te_3 presented a saturable absorption at the laser wavelengths of 532 and 1064 nm with the lowest incident energy of 8.5 and 20 μJ. The reason is that the energy band gap of Bi_2Te_3 (~0.16 eV) is much smaller than the energy of 532 nm (2.33 eV) and 1064 nm (1.164 eV) photons, thus pointing out that the Bi_2Te_3 nanosheets can be easily excited at the used laser wavelengths. In addition, their OA Z-scan curves of Bi_2Te_3 nanocrystals have shown that a valley within the peak at the focus point becomes deeper with the growth of the input energies from 21 to 51 μJ at 532 nm and from 42 to 69 μJ at 1064 nm. The β of Bi_2Te_3 increased from the negative values (−80 cm GW^{-1}) to 880 cm GW^{-1} and from −50 to 230 cm GW^{-1} when the input energies increase from 8.5 to 51 μJ at 532 nm and from 20 to 69 μJ at 1064 nm, respectively. At high intensities, the third-order nonlinearities primarily include the two-photon absorption and nonlinear scattering [4]. The larger the input intensities are, the stronger the two-photon effect and the thermally-induced nonlinear scattering effect were manifested at their conditions. In our case (150 fs PP), these effects were not observed.

A mode-locked erbium-doped fiber laser (1562 nm, 1.5 ps, 20.8 MHz) and a mode-locked ytterbium-doped fiber laser (1060 nm, 130 ps, 2.7 MHz) were used in [3] as laser sources for

Optics EXPRESS

the OA Z-scans to characterize the nonlinear absorption of Bi_2Te_3 nanocrystals at different wavelengths. The saturation intensity was determined to be very low ($\sim 10^5$ W cm^{-2} at both 1562 and 1060 nm). Overall, the Bi_2Te_3 nanocrystals showed the variable nonlinear optical response, which is attributed to the different wavelength, pulse duration, and the available laser sources adopted with different operating parameters, particularly, pulse repetition rates. For example, in our case, we observed the notably larger I_{sat} at 1000 nm in the case of femtosecond pulses ($\sim 10^8$ W cm^{-2}, Fig. 6(b)). Thus the above analysis shows a broad range of the variations of the nonlinear optical parameters of Bi_2Te_3 nanocrystals reported by different groups of researchers.

5. Conclusions

We have measured the nonlinear optical parameters of synthesized Bi_2Te_3 nanoparticles-contained thin films using the tunable femtosecond laser in the range of 400–1000 nm. We have shown that these nanoparticles-contained films possess strong saturable absorption and positive nonlinear refraction (-6.8×10^{-5} cm W^{-1} in the case of 500 nm, 150 fs probe pulses, and 3×10^{-10} cm^2 W^{-1} in the case of 400 nm, 150 fs probe pulses, respectively). The spectral, intensity, and temporal variation of saturable absorption and nonlinear refraction of the thin films containing exfoliated Bi_2Te_3 nanoparticles are discussed. The measurements of saturable absorption have shown that these films containing exfoliated Bi_2Te_3 NPs possess low values of the saturated intensity ($I_{sat} = 3.2\times10^{10}$ W cm^{-2}). Such low-I_{sat} saturable absorbers may allow the formation of low-power femtosecond laser sources. Finally, we compared the nonlinear optical parameters of these films measured by femtosecond and nanosecond pulses.

Funding. Horizon 2020 Framework Programme (739508, project CAMART^2); Russian Foundation for Basic Research (18-29-20080); European Regional Development Fund (1.1.1.5/19/A/003).

Acknowledgment. Institute of Solid State Physics, University of Latvia as the Center of Excellence acknowledges funding from the European Union's Horizon 2020 Framework Programme H2020-WIDESPREAD-01-2016-2017-TeamingPhase2 under grant agreement No. 739508, project CAMART^2.

Disclosures. The authors declare no conflict of interest.

Data availability. Data underlying the results presented in this paper are not publicly available at this time but may be obtained from the authors upon reasonable request.

References

1. J. Yao, K. J. Koski, W. Luo, J. J. Cha, L. Hu, D. Kong, V. K. Narasimhan, K. Huo, and Y. Cui, "Optical transmission enhacement through chemically tuned two-dimensional bismuth chalcogenide nanoplates," Nat. Commun. **5**(1), 5670 (2014).
2. Y. Lin, S. Lin, Y. Chi, C. Wu, C. Cheng, W. Tseng, J. He, C. Wu, C. Lee, and G. Lin, "Using n-and p-type Bi_2Te_3 topological insulator nanoparticles to enable controlled femtosecond mode-locking of fiber lasers," ACS Photonics **2**(4), 481–490 (2015).
3. G. Jiang, J. Yi, L. Miao, P. Tang, H. Huang, C. Zhao, and S. Wen, "Bismuth Telluride nanocrystal: broadband nonlinear response and its application in ultrafast photonics," Sci. Rep. **8**(1), 2355 (2018).
4. J. Qiao, M.-Y. Chuang, J.-C. Lan, Y.-Y. Lin, W.-H. Sung, R. Fan, M.-Y. Wu, C.-Y. Lee, C.-H. Chen, H. Liu, and C.-K. Lee, "Two-photon absorption within layered Bi_2Te_3 topological insulators and the role of nonlinear transmittance therein," J. Mater. Chem. C **7**(23), 7027–7034 (2019).
5. J.-C. Lan, J. Qiao, W.-H. Sung, C.-H. Chen, R.-H. Jhang, S.-H. Lin, L.-R. Ng, G. Liang, M.-Y. Wu, L.-W. Tu, C.-M. Cheng, H. Liu, and C.-K. Lee, "Role of carrier-transfer in the optical nonlinearity of graphene/Bi_2Te_3 heterojunctions," Nanoscale **12**(32), 16956–16966 (2020).
6. D. Liu, C. He, L. Chen, W. Li, and Y. Zu, "The nonlinear absorption effects and optical limiting properties of Bi_2Te_3/rGO thin films," Opt. Mater. **111**, 110634 (2021).
7. L. Miao, J. Yi, Q. Wang, D. Feng, H. He, S. Lu, C. Zhao, H. Zhang, and S. Wen, "Broadband third order nonlinear optical responses of bismuth telluride nanosheets," Opt. Mater. Express **6**(7), 2244–2251 (2016).
8. R. A. Ganeev, V. S. Popov, A. I. Zvyagin, N. A. Lavrentyev, A. E. Mirofyanchenko, E. V. Mirofyanchenko, I. A. Shuklov, O. V. Ovchinnikov, V. P. Ponomarenko, and V. F. Razumov, "Exfoliated Bi_2Te_3 nanoparticle suspensions and films: morphological and nonlinear optical characterization," Nanophotonics **10**(15), 3857–3870 (2021).
9. V. S. Popov, A. V. Egorov, and V. P. Ponomarenko, "Obtaining photosensitive elements based on two-dimensional bismuth telluride and their volt-ampere characteristics," Appl. Phys. **5**, 50–55 (2020).

Optics EXPRESS

10. V. S. Popov, A. V. Egorov, and V. P. Ponomarenko, "Photosensitive elements based on two-dimensional bismuth telluride: obtaining and current–voltage characteristics," J. Commun. Technol. Electron. **66**(9), 1092–1095 (2021).
11. C. Bauer, I. Veremchuk, C. Kunze, A. Benad, V. M. Dzhagan, D. Haubold, D. Pohl, G. Schierning, K. Nielsch, V. Lesnyak, and A. Eychmüller, "Heterostructured bismuth telluride selenide nanosheets for enhanced thermoelectric performance," Small Sci. **1**(1), 2000021 (2021).
12. H. Bando, K. Koizumi, Y. Oikawa, K. Daikohara, V. A. Kulbachinskii, and H. Ozaki, "The time-dependent process of oxidation of the surface of Bi_2Te_3 studied by X-ray photoelectron spectroscopy," J. Phys.: Condens. Matter **12**(26), 5607–5616 (2000).
13. X. Liu, S. Guo, H. Wang, and L. Hou, "Theoretical study on the closed-aperture Z-scan curves in the materials with nonlinear refraction and strong nonlinear absorption," Opt. Commun. **197**(4-6), 431–437 (2001).
14. M. Sheik-Bahae, A. A. Said, T. H. Wei, D. J. Hagan, and E. W. Van Stryland, "Sensitive measurement of optical nonlinearities using a single beam," IEEE J. Quantum Electron. **26**(4), 760–769 (1990).
15. L. R. Brovelli, U. Keller, and H. H. Chiu, "Design and operation of antiresonant Fabry−Perot saturable semiconductor absorbers for mode-locked solid-state lasers," J. Opt. Soc. Am. B **12**(2), 311–322 (1995).
16. P. T. Guerreiro, S. Ten, N. F. Borrelli, J. Butty, G. E. Jabbour, and N. Peyghambarian, "PbS quantum-dot doped glasses as saturable absorbers for mode locking of a Cr:forsterite laser," Appl. Phys. Lett. **71**(12), 1595–1597 (1997).
17. A. M. Malyarevich, V. G. Savitski, P. V. Prokoshin, N. N. Posnov, K. V. Yumashev, E. Raaben, and A. A. Zhilin, "Glass doped with PbS quantum dots as a saturable absorber for 1-μm neodymium lasers," J. Opt. Soc. Am. B **19**(1), 28–32 (2002).
18. V. P. Ponomarenko, V. S. Popov, S. V. Popov, and E. L. Chepurnov, "Photo- and nanoelectronics based on two-dimensional materials. Part I. Two-dimensional materials: properties and synthesis," J. Commun. Technol. Electron. **65**(9), 1062–1104 (2020).
19. J. Li, H. Luo, L. Wang, C. Zhao, H. Zhang, H. Li, and Y. Liu, "3-μm mid-infrared pulse generation using topological insulator as the saturable absorber," Opt. Lett. **40**(15), 3659–3662 (2015).
20. P. H. Tang, M. Wu, Q. K. Wang, L. L. Miao, B. Huang, J. Liu, C. J. Zhao, and S. C. Wen, "2.8 μm-pulsed Er^{3+}:ZBLAN fiber laser modulated by topological insulator," IEEE Photonics Technol. Lett. **28**(14), 1573–1576 (2016).
21. C. J. Zhao, H. Zhang, X. Qi, Y. Chen, Z. T. Wang, S. C. Wen, and D. Y. Tang, "Ultra-short pulse generation by a topological insulator based saturable absorber," Appl. Phys. Lett. **101**(21), 211106 (2012).
22. J. Sotor, G. Sobon, W. Macherzynski, P. Paletko, K. Grodecki, and K. M. Abramski, "Mode-locking in Er-doped fiber laser based on mechanically exfoliated Sb_2Te_3 saturable absorber," Opt. Mater. Express **4**(1), 1–6 (2014).
23. Z. C. Luo, M. Liu, H. Liu, X. W. Zheng, A. P. Luo, C. J. Zhao, H. Zhang, S. C. Wen, and W. C. Xu, "2 GHz passively harmonic mode-locked fiber laser by a microfiber-based topological insulator saturable absorber," Opt. Lett. **38**(24), 5212–5215 (2013).
24. Z. Yue, Q. Chen, A. Sahu, X. Wang, and M. Gu, "Photo-oxidation-modulated refractive index in Bi_2Te_3 thin films," Mater. Res. Express **4**(12), 126403 (2017).
25. M. Saleemi, M. S. Toprak, S. Li, M. Johnsson, and M. Muhammed, "Synthesis, processing, and thermoelectric properties of bulk nanostructured bismuth telluride (Bi_2Te_3)," J. Mater. Chem. **22**(2), 725–730 (2012).